Drug Delivery

DOI: 10.1002/anie.201400268

Enhanced Anticancer Efficacy by ATP-Mediated Liposomal Drug Delivery**

Ran Mo, Tianyue Jiang, and Zhen Gu**

Abstract: *A liposome-based co-delivery system composed of a fusogenic liposome encapsulating ATP-responsive elements with chemotherapeutics and a liposome containing ATP was developed for ATP-mediated drug release triggered by liposomal fusion. The fusogenic liposome had a protein–DNA complex core containing an ATP-responsive DNA scaffold with doxorubicin (DOX) and could release DOX through a conformational change from the duplex to the aptamer/ATP complex in the presence of ATP. A cell-penetrating peptide-modified fusogenic liposomal membrane was coated on the core, which had an acid-triggered fusogenic potential with the ATP-loaded liposomes or endosomes/lysosomes. Directly delivering extrinsic liposomal ATP promoted the drug release from the fusogenic liposome in the acidic intracellular compartments upon a pH-sensitive membrane fusion and anticancer efficacy was enhanced both in vitro and in vivo.*

Stimuli-responsive drug-delivery systems (DDSs) are playing an increasingly crucial role in a diverse spectrum of applications for disease treatment.[1] These environmental stimuli involve external triggers,[2] such as temperature,[2a] light,[2b] magnetic field,[2c] ultrasound,[2d] electric current,[2e] radio waves,[2f] and γ radiation,[2g] as well as internal factors, such as pH,[3] redox reactions,[4] enzymatic expression,[5] glucose levels,[6] and the presence of reactive oxygen species.[7] Nanoparticle (NP)-based DDSs including liposomes, polymeric NPs, and protein/DNA-based nanocarriers have been extensively investigated to respond to these signals for delivery of their cargoes in an on-demand fashion.[8]

Adenosine-5′-triphosphate (ATP), the essential biogenic biomolecule for cellular energy metabolism and signaling, is highly present within the cells at a concentration range of 1-10 mM, much greater than that of ATP in the extracellular environment (<5 μM).[9] The distinct difference in the ATP levels between extracellular and intracellular milieu is the biological principle for the design of ATP-responsive carriers, which is recently attracting considerable interest.[10]

We herein report a liposome-based co-delivery system consisting of a fusogenic liposome encapsulating ATP-responsive elements and a liposome containing ATP for ATP-triggered drug release mediated by the liposomal fusion. The fusogenic liposome contains a protein–DNA complex core, which is composed of protamine and an ATP-responsive DNA scaffold (Figure 1a). The DNA segment was composed of the duplex hybridized by the ATP aptamer and its complementary single-stranded DNA (cDNA), which shows a specific and high affinity to ATP and has been often utilized for ATP detection.[11] Doxorubicin (DOX), a model small-molecule anticancer drug that is particularly prone to be intercalated in the GC pair of DNA motif, is applied to form the DOX-loaded duplex (DOX-Duplex).[12] The interaction of the complex of the ATP aptamer with ATP results in the dissociation of the DNA duplex and the liberation of cDNA, which thereby causes the release of the intercalated DOX from DOX-Duplex through a structural transformation[10c] from the duplex to the aptamer/ATP complex (Figure 1b). The cationic protamine is employed to condense the anionic DNA scaffold to a complex (DOX-Complex), which has cell-penetrating and nucleus-targeting capabilities.[13] A liposomal membrane modified with a cell-penetrating peptide (CPP, R6H4) and having the fusogenic lipid composition of dioleoylphosphatidylethanolamine (DOPE) is coated on the core complex to obtain the DOX-Duplex-loaded fusogenic liposomes (DOX-FL), which have an acid-triggered fusogenic potential with the ATP-loaded liposomes (ATP-L) or endosomes/lysosomes (endo-lysosomes).[14]

As illustrated in Figure 1c, after internalization by the tumor cells, DOX-FL and ATP-L are expected to be localized in the endo-lysosomes. In these intracellular acidic compartments, the membrane fusion of DOX-FL with ATP-L is induced due to the pH-sensitive fusogenic potential of DOPE enhanced by the R6H4 peptide, which leads to the exposure of DOX-Duplex to co-delivered ATP and subsequently triggers the release of intercalated DOX. Meanwhile, DOX-FL also possesses fusogenic activity with the endo-lysosomal membranes, thereby promoting endo-lysosomal escape and facilitating the transport of the released DOX to the cytosol, where it then specifically accumulates in the nuclei to eventually trigger cytotoxicity and apoptosis. This co-delivery system provides a new strategy for intracellular ATP-triggered drug release, which can be tuned by the direct delivery

[*] Dr. R. Mo, T. Jiang, Prof. Dr. Z. Gu
Joint Department of Biomedical Engineering
University of North Carolina at Chapel Hill
and North Carolina State University
Raleigh, NC 27695 (USA)
and
Molecular Pharmaceutics Division
Eshelman School of Pharmacy
University of North Carolina at Chapel Hill
Chapel Hill, NC 27599 (USA)
E-mail: rmo@ncsu.edu
zgu@email.unc.edu
zgu3@ncsu.edu

[**] This work was supported by NC TraCS (grant 550KR51307), NIH's Clinical and Translational Science Awards (CTSA, 1UL1TR001111) at UNC-CH, the NC State Faculty Research and Professional Development Award, and the start-up package from the Joint BME Department of UNC-CH and NCSU to Z.G.

Supporting information for this article is available on the WWW under http://dx.doi.org/10.1002/anie.201400268.

 © 2014 Wiley-VCH Verlag GmbH & Co. KGaA, Weinheim

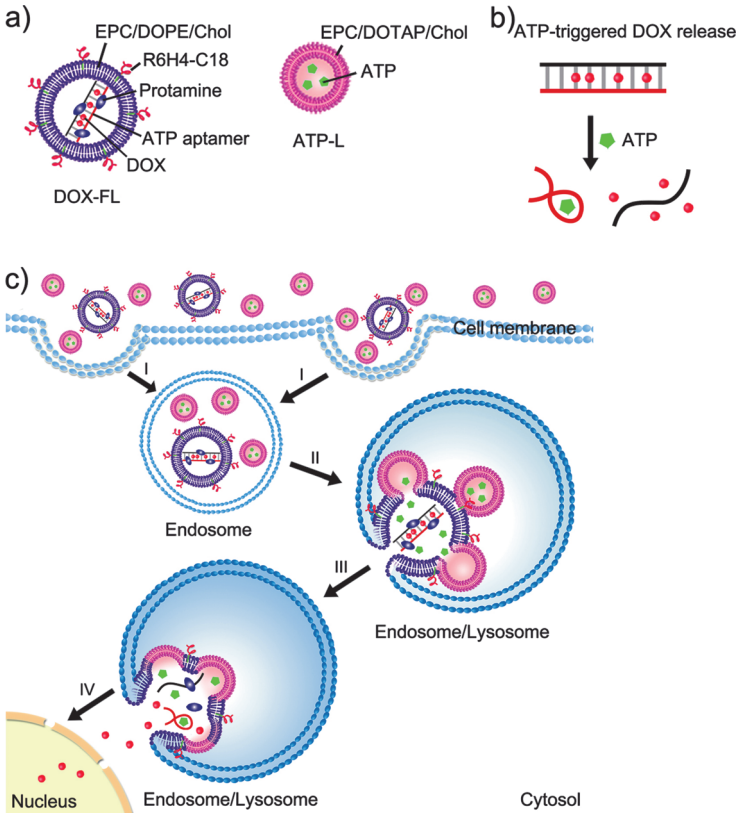

Figure 1. a) Main components of DOX-FL and ATP-L. DOX-FL has an ATP-responsive protein–DNA complex core with DOX and a pH-sensitive CPP-modified fusogenic liposomal shell. b) Mechanism of ATP-triggered release of DOX through the structural transformation from the duplex to the aptamer/ATP complex. c) Schematic illustration of ATP-responsive co-delivery of DOX-FL and ATP-L. I: internalization of DOX-FL and ATP-L in endosomes; II: pH-responsive membrane fusion of DOX-L with ATP-L and endo-lysosomes; III: ATP-triggered DOX release; IV: accumulation of DOX in the cell nucleus. EPC = egg phosphatidylcholine, DOPE = 1,2-dioleoyl-*sn*-glycero-3-phosphoethanolamine, Chol = cholesterol, DOTAP = 1,2-dioleoyl-3-trimethylammoniumpropane.

of ATP molecules or other relevant metabolic elements as external regulators.

To validate our assumption, we first developed the ATP-responsive DNA scaffold by hybridizing the ATP aptamer and its cDNA, which was used for DOX loading. The fluorescence intensity of DOX showed a sequential reduction when DOX at a fixed concentration was incubated with an increasing mass ratio of the DNA duplex (Figure 2a and Figure S1 in the Supporting Information), which was attributed to the occurrence of Förster resonance energy transfer (FRET) between the DOX molecules intercalating in the duplex.[10c, 12b] The trend reached a maximum in the quenching efficiency at the duplex/DOX mass ratio of 10:1. To evaluate the ATP-responsive release of DOX from the duplex, DOX-Duplex was incubated with different concentrations of ATP. The release of DOX due to the dissociation of the duplex in the presence of ATP can be judged by the recovery of the DOX fluorescence signal. DOX-Duplex presented an ATP-concentration-dependent DOX fluorescence recovery. The relative DOX fluorescence intensity showed a concomitant increase with the ATP concentration (Figure 2b). In contrast, the *R* values of DOX-Duplex had insignificant variation when DOX-Duplex was incubated with the ATP analogues, including guanosine triphosphate (GTP), cytidine triphosphate (CTP), and uridine triphosphate (UTP).

Next, we mixed DOX-Duplex with protamine at a mass ratio of 0.7:1 to form a negatively charged DOX-Complex (Figure S2 in the Supporting Information).[13] The complex was then added with positively charged R6H4-modified fusogenic liposome (R6H4-FL) at a lipid to duplex molar ratio of of 80:1 (Figure S3 in the Supporting Information), followed by gentle ultrasonication and incubation to achieve DOX-FL.[15] The DOX fluorescence was also quenched in the obtained DOX-FL (Figure S4 in the Supporting Information). The changes in the particle size and zeta potential during the development of DOX-FL indicated the encapsulation of the liposomal membrane on the complex and the fabrication of DOX-FL (Figure S5 in the Supporting Information), which had a hydrodynamic diameter of about 195 nm and a zeta potential of +16 mV. Transmission electron microscope (TEM) images indicated that the particle size of DOX-FL was around 180 nm (Figure S6 in the Supporting Information). Confocal laser scanning microscope (CLSM) images of nitrobenzyloxadiazole (NBD)-labeled DOX-FL showed colocalization of the red DOX signal with the green NBD signal (Figure S7 in the Supporting Information). We also prepared ATP-L with a drug-loading capacity of approximately 16.7% using the freeze–thaw method;[16] the ATP-L particles had a diameter of about 100 nm (Figure S8 in the Supporting Information) and a zeta potential

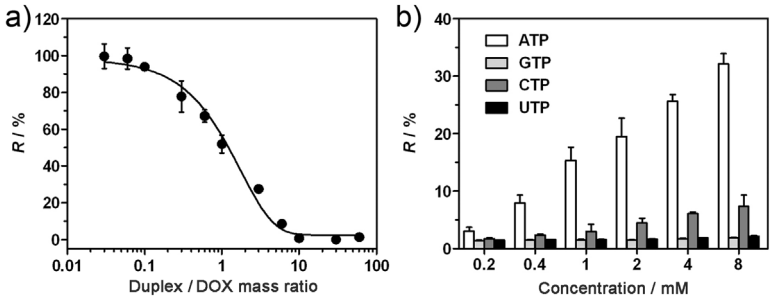

Figure 2. a) Relative DOX fluorescence intensity (*R*) of DOX-Duplex (0.5 μg mL^{-1}) at different duplex/DOX mass ratios in HEPES buffer (5 mM). b) Relative DOX fluorescence intensity (*R*) of DOX-Duplex (0.5 μg mL^{-1}) at the duplex/DOX mass ratio of 10:1 in the presence of different concentrations of ATP, GTP, UTP, and CTP in HEPES buffer (5 mM) containing 10 mM $MgCl_2$ and 100 mM NaCl. Data points represent mean ± SD ($n = 3$). *R* is denoted as $(I_{NTP} - I_0)/(I - I_0) \times 100\%$, where *I* is the fluorescence intensity of DOX in solution without the duplex, I_{NTP} and I_0 are the fluorescence intensities of DOX in DOX-Duplex at the DOX concentration equivalent to that of the DOX solution in the presence and absence of the NTPs ATP, GTP, CTP, and UTP, respectively.

© 2014 Wiley-VCH Verlag GmbH & Co. KGaA, Weinheim

of +3 mV. Compared with ATP-L, DOX-FL showed an increase in positive surface charges due to a gradual protonation of imidazole groups in R6H4 at lower pH (Figure S9 in the Supporting Information).

To explore the fusogenic potential between R6H4-FL and endo-lysosomes, we used anionic liposomes composed of biomembrane-mimicking lipids to simulate the endo-lysosomes, which were double-labeled with a FRET donor–acceptor pair. Liposome fusion was monitored using a standard FRET assay.[17] R6H4-FL showed higher fusogenic capabilities at low pH values (Figure 3a). After 1 h incubation, the fusogenic potential was about 22% at pH 5.5 and 32% at pH 4.5, significantly higher than 12% at pH 7.4. It was indicated that higher acidity of the endo-lysosomes promoted its membrane fusion with R6H4-FL, which resulted in the escape of the payload from the endo-lysosomes. Moreover, compared with the R8-modified fusogenic liposome (R8-FL), R6H4-FL displayed an enhanced pH-buffering capacity from neutral to acidic conditions (Figure S10 in the Supporting Information); this is similar to the buffering capacity of other liposomes with histidine lipids,[18] also known as the proton sponge effect for endo-lysosomal escape. To further investigate the fusion between DOX-FL and ATP-L, DOX-FL was incubated with ATP-L at different pH values. The liposomal fusion allows the exposure of DOX-Duplex to ATP and subsequently leads to ATP-triggered DOX release from DOX-Duplex, which can be estimated by detecting the recovery of the DOX fluorescence. A remarkable recovery of DOX fluorescence was observed after DOX-FL incubation with ATP-L at higher acidities compared to that at neutral pH (Figure 3b). Accordingly, DOX-FL had an acidity-enhancing effect on fusion with endo-lysosomes and ATP-L for endo-lysosomal escape and ATP-responsive DOX release, respectively, which resulted from the fusogenic lipid DOPE and highly positive surface charge provided by R6H4 in the acidic endo-lysosomes.

A further investigation of the release of DOX from DOX-FL in the presence and absence of ATP-L was conducted using a dialysis tube (Figure 3c). The pH decrease had a certain contribution to the DOX release even when DOX-FL was incubated with the blank liposomes (Blank-L) without ATP, which was due to the higher solubility of protonated DOX under acidic conditions. By comparison, the presence of ATP-L significantly accelerated the release of DOX from DOX-FL at the lower pH values (Figure 3d), where fusion of DOX-FL with ATP-L was promoted, followed by the fast release of the intercalated DOX molecules under high ATP levels.

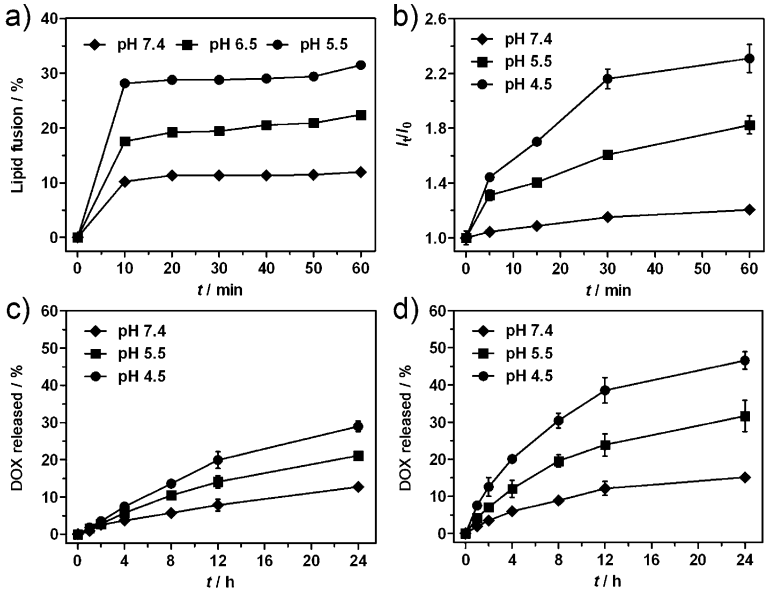

Figure 3. a) Fusogenic potential of R6H4-FL with anionic liposomes with an endo-lysosome-mimicking membrane at different pH values over time. Data points represent mean ±SD ($n=2$). b) Fusogenic potential of DOX-FL with ATP-L at different pH values over time. I_t and I_0 are the fluorescence intensities of DOX before and after incubation for different times, respectively. Data points represent mean ±SD ($n=2$). c, d) In vitro release profiles of DOX from DOX-FL without (c) and with ATP-L (d) at different pH values. Data points represent mean ±SD ($n=3$).

The intracellular trafficking profile of this co-delivery system was evaluated by CLSM. Human breast cancer (MCF-7) cells were incubated with a mixture of DOX-FL and NBD-labeled ATP-L (NBD-ATP-L) for different time periods (Figure 4a and Figure S11 in the Supporting Information). As the incubation time increased from 0.5 to 2 h, DOX-FL (red) and NBD-ATP-L (green) were effectively internalized by the cells and colocalized into the endo-lysosomes (blue), judged by the increased white pixels. The colocalization ratio between DOX and the endo-lysosomal marker LysoTracker increased from 29% to 80% (Figure 4b), which was an indicator for endo-lysosomal entrapment. After 2 h incubation, the excess liposomes were removed and the cells were then incubated with fresh culture media for an additional 1, 2, or 4 h. The separation in the signals of DOX, NBD, and LysoTracker was observed, determined by the decreased white and increased individual color pixels (Figure 4a). The colocalization ratio of DOX with LysoTracker reduced to 24% after an additional 4 h of incubation (Figure 4b), which suggested the efficient endo-lysosomal escape of DOX due to the membrane fusion between DOX-FL and endo-lysosomes along with the proton sponge effect of DOX-FL. In addition, the colocalization ratio of DOX with NBD decreased from 88% to 18%, and the co-delivery of DOX-FL with ATP-L showed the increased release of DOX in the cells compared with that of DOX-FL with Blank-L (Figure 3c), indicating that a significant part of DOX-FL fused with ATP-L and activated the ATP-mediated release of the encapsulated DOX in the cells. Furthermore, the released DOX was clearly visualized in the nuclei after an additional 2 h of incubation, and increased considerably as the incubation time extended to 4 h (Figure 4a), which implied the efficient nucleus-targeting of the released DOX.

The in vitro cytotoxicity of co-delivery of DOX-FL with ATP-L against MCF-7 cells was estimated using the 3-(4,5-

 © 2014 Wiley-VCH Verlag GmbH & Co. KGaA, Weinheim

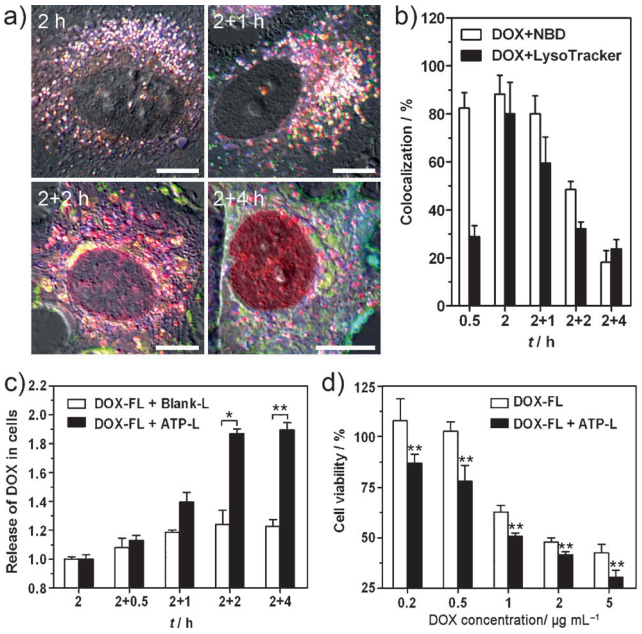

Figure 4. a) CLSM images of MCF-7 cells after incubation with DOX-FL and NBD-ATP-L for different times. The cells were incubated with a mixture of DOX-FL and NBD-ATP-L for 2 h, and subsequently incubated with fresh culture medium for an additional 1, 2, or 4 h after removal of the excess liposomes. Late endosomes and lysosomes were stained by LysoTracker Blue. Red: DOX; green: NBD; blue: endo-lysosomes; yellow: colocalization of red and green pixels; magenta: colocalization of red and blue pixels; white: colocalization of red, green, and blue pixels. Scale bars are 10 μm. b) Time-dependent changes in colocalization ratios between DOX and NBD or endo-lysosomes. Data points represent mean ± SD ($n = 5$). c) The release of DOX from DOX-FL co-delivered with ATP-L or Blank-L in MCF-7 cells obtained using flow cytometry. The DOX release ratio is determined by comparing the fluorescence intensity of DOX after 2 h of incubation and that after an additional 0.5, 1, 2 or 4 h of incubation. Data points represent mean ± SD ($n = 2$). $*P < 0.05$, $**P < 0.01$. d) In vitro cytotoxicity of co-delivery of DOX-FL and ATP-L toward MCF-7 cells. Data points represent mean ± SD ($n = 6$). $**P < 0.01$.

dimethylthiazol-2-yl)-2,5-diphenyltetrazolium bromide (MTT) assay (Figure 4d). The half-maximal inhibitory concentration (IC_{50}) of DOX-FL co-delivered with ATP-L was calculated to be 1.5 μg mL^{-1} with MCF-7 cells, noticeably lower than the value of 2.6 μg mL^{-1} of DOX-FL alone. The blank R6H4-FL without DOX, ATP-L, and their mixture did not show significant toxicities at the tested range of concentrations (Figure S12 in the Supporting Information). Collectively, the intracellular release of DOX from DOX-FL enhanced by ATP-L supported higher cytotoxic efficacy toward the cancer cells.

We then applied a model (MCF-7 cancer xenograft nude mice) to evaluate the retention capacities of the liposome-based co-delivery system in tumor tissue. The signal of DOX delivered by DOX-FL in the frozen tumor sections was prominently higher than that of the DOX solution, which could still be observed even at 72 h post-injection (Figure S13 in the Supporting Information). In contrast, the relevant signal from samples associated with the DOX solution almost disappeared at 48 h post-injection. It was validated that DOX-FL extended the tumor residence of the DOX molecule partially due to enhanced tumor penetration and cellular uptake upon R6H4 modification on the liposomal surface, while the DOX solution was subject to a more rapid clearance from the tumor tissue. In addition, C6-loaded liposomes with the same lipid composition as ATP-L maintained the C6 signals at the tumor site for more than 48 h.

Next, the in vivo antitumor efficacy of the co-delivery system was investigated. After intratumoral injection, different DOX formulations significantly inhibited the tumor growth of the mice relative to that of mice injected with saline (Figure 5). DOX-FL with and without ATP-L both

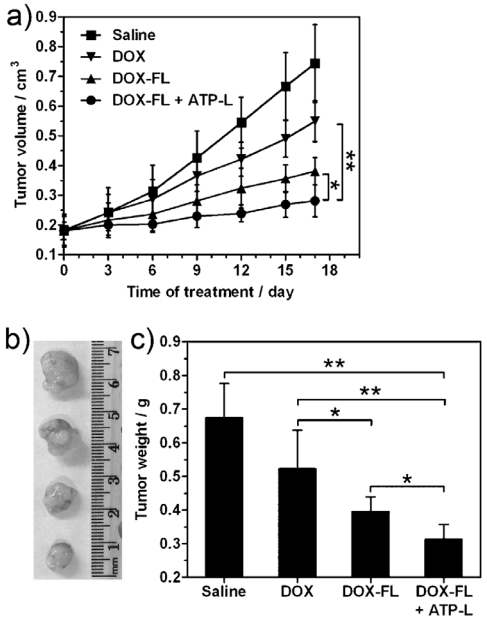

Figure 5. a) Tumor growth curves of the tumor-bearing mice after intratumoral injection with different DOX formulations. b) Representative images of the tumors collected from the mice at Day 17 (from top to bottom: saline, DOX, DOX-FL, DOX-FL with ATP-L). c) Weights of the tumors collected from the mice at Day 17. Data points represent mean ± SD ($n = 5$). $*P < 0.05$, $**P < 0.01$.

showed remarkably higher inhibition effects toward tumor growth than the DOX solution, which was due to the enhanced tumor retention capabilities of DOX-FL decorated with R6H4. Of note, DOX-FL co-delivered with ATP-L showed a noticeable difference in tumor-size inhibition compared to that of DOX-FL alone, indicating that the extrinsic ATP played an effective role in the DOX release. Meanwhile, no significant change in the body weight of the mice was found during the treatment (Figure S14 in the Supporting Information). Additionally, the histologic images stained by the hematoxylin and eosin (HE) exhibited a massive cancer cell remission in the tumor tissue of the mice receiving DOX-FL with ATP-L (Figure S15, Supporting Information). Furthermore, the terminal deoxynucleotidyl transferase dUTP nick end labeling (TUNEL) imaging assay showed the highest level of apoptotic DNA fragmentation stained by the AlexaFluor 488 (green) (Figure S16 in the

 © 2014 Wiley-VCH Verlag GmbH & Co. KGaA, Weinheim

Supporting Information). Besides intratumoral injection, passively targeting-based co-delivery of DOX-FL with ATP-L by intravenous administration also showed promising tumor growth inhibition effects compared with that of the DOX solution and DOX-FL (Figure S17 in the Supporting Information).

In summary, we have developed an ATP-responsive drug-delivery system consisting of a protein–DNA core and a CPP-modified fusogenic liposomal shell, which presents drug-release behaviors associated with the surrounding ATP levels. Direct delivery of liposomal ATP promoted the release of drug from the liposome mediated by the pH-sensitive liposomal fusion in the intracellular acidic compartments, which showed an enhanced therapeutic efficacy in cancer therapy.[19]

Received: January 10, 2014
Published online: April 24, 2014

Keywords: ATP · drug delivery · liposomes · nanomedicine · stimuli-responsive materials

[1] a) S. Mura, J. Nicolas, P. Couvreur, *Nat. Mater.* **2013**, *12*, 991 – 1003; b) Z. Ge, S. Liu, *Chem. Soc. Rev.* **2013**, *42*, 7289 – 7325; c) M. Motornov, Y. Roiter, I. Tokarev, S. Minko, *Prog. Polym. Sci.* **2010**, *35*, 174 – 211.

[2] a) S. W. Choi, Y. Zhang, Y. Xia, *Angew. Chem.* **2010**, *122*, 8076 – 8080; *Angew. Chem. Int. Ed.* **2010**, *49*, 7904 – 7908; b) H. I. Lee, W. Wu, J. K. Oh, L. Mueller, G. Sherwood, L. Peteanu, T. Kowalewski, K. Matyjaszewski, *Angew. Chem.* **2007**, *119*, 2505 – 2509; *Angew. Chem. Int. Ed.* **2007**, *46*, 2453 – 2457; c) H. Oliveira, E. Perez-Andres, J. Thevenot, O. Sandre, E. Berra, S. Lecommandoux, *J. Controlled Release* **2013**, *169*, 165 – 170; d) S. Hernot, A. L. Klibanov, *Adv. Drug Delivery Rev.* **2008**, *60*, 1153 – 1166; e) I. C. Kwon, Y. H. Bae, S. W. Kim, *Nature* **1991**, *354*, 291 – 293; f) S. A. Stanley, J. E. Gagner, S. Damanpour, M. Yoshida, J. S. Dordick, J. M. Friedman, *Science* **2012**, *336*, 604 – 608; g) W. Cao, X. Zhang, X. Miao, Z. Yang, H. Xu, *Angew. Chem.* **2013**, *125*, 6353 – 6357; *Angew. Chem. Int. Ed.* **2013**, *52*, 6233 – 6237.

[3] a) Y. Lee, T. Ishii, H. Cabral, H. J. Kim, J. H. Seo, N. Nishiyama, H. Oshima, K. Osada, K. Kataoka, *Angew. Chem.* **2009**, *121*, 5413 – 5416; *Angew. Chem. Int. Ed.* **2009**, *48*, 5309 – 5312; b) C. J. Ke, T. Y. Su, H. L. Chen, H. L. Liu, W. L. Chiang, P. C. Chu, Y. Xia, H. W. Sung, *Angew. Chem.* **2011**, *123*, 8236 – 8239; *Angew. Chem. Int. Ed.* **2011**, *50*, 8086 – 8089; c) H. Takemoto, K. Miyata, S. Hattori, T. Ishii, T. Suma, S. Uchida, N. Nishiyama, K. Kataoka, *Angew. Chem.* **2013**, *125*, 6338 – 6341; *Angew. Chem. Int. Ed.* **2013**, *52*, 6218 – 6221; d) P. Moitra, K. Kumar, P. Kondaiah, S. Bhattacharya, *Angew. Chem.* **2014**, *126*, 1131 – 1135; *Angew. Chem. Int. Ed.* **2014**, *53*, 1113 – 1117.

[4] a) W. Ong, Y. Yang, A. C. Cruciano, R. L. McCarley, *J. Am. Chem. Soc.* **2008**, *130*, 14739 – 14744; b) M. Zhao, B. Hu, Z. Gu, K.-I. Joo, P. Wang, Y. Tang, *Nano Today* **2013**, *8*, 11 – 20; c) X. Wang, X. Cai, J. Hu, N. Shao, F. Wang, Q. Zhang, J. Xiao, Y. Cheng, *J. Am. Chem. Soc.* **2013**, *135*, 9805 – 9810.

[5] a) Z. Gu, M. Yan, B. Hu, K. I. Joo, A. Biswas, Y. Huang, Y. Lu, P. Wang, Y. Tang, *Nano Lett.* **2009**, *9*, 4533 – 4538; b) A. Biswas, K.-I. Joo, J. Liu, M. Zhao, G. Fan, P. Wang, Z. Gu, Y. Tang, *ACS Nano* **2011**, *5*, 1385 – 1394; c) R. Toita, J. H. Kang, T. Tomiyama, C. W. Kim, S. Shiosaki, T. Niidome, T. Mori, Y. Katayama, *J. Am. Chem. Soc.* **2012**, *134*, 15410 – 15417; d) T. Jiang, R. Mo, A. Bellotti, J. Zhou, Z. Gu, *Adv. Funct. Mater.* **2014**, DOI: 10.1002/adfm.201303222.

[6] a) Z. Gu, A. A. Aimetti, Q. Wang, T. T. Dang, Y. Zhang, O. Veiseh, H. Cheng, R. S. Langer, D. G. Anderson, *ACS Nano* **2013**, *7*, 4194 – 4201; b) A. Matsumoto, T. Ishii, J. Nishida, H. Matsumoto, K. Kataoka, Y. Miyahara, *Angew. Chem.* **2012**, *124*, 2166 – 2170; *Angew. Chem. Int. Ed.* **2012**, *51*, 2124 – 2128; c) S. Wu, X. Huang, X. Du, *Angew. Chem.* **2013**, *125*, 5690 – 5694; *Angew. Chem. Int. Ed.* **2013**, *52*, 5580 – 5584; d) Y. Zhao, B. G. Trewyn, I. I. Slowing, V. S. Lin, *J. Am. Chem. Soc.* **2009**, *131*, 8398 – 8400; e) R. Mo, T. Jiang, J. Di, W. Tai, Z. Gu, *Chem. Soc. Rev.* **2014**, DOI: 10.1039/C3CS60436E.

[7] a) M. S. Shim, Y. Xia, *Angew. Chem.* **2013**, *125*, 7064 – 7067; *Angew. Chem. Int. Ed.* **2013**, *52*, 6926 – 6929; b) C. de Gracia Lux, S. Joshi-Barr, T. Nguyen, E. Mahmoud, E. Schopf, N. Fomina, A. Almutairi, *J. Am. Chem. Soc.* **2012**, *134*, 15758 – 15764; c) B. S. Lee, T. Amano, H. Q. Wang, J. L. Pantoja, C. W. Yoon, C. J. Hanson, R. Amatya, A. Yen, K. L. Black, J. S. Yu, *ACS Nano* **2013**, *7*, 3061 – 3077.

[8] a) D. Peer, J. M. Karp, S. Hong, O. C. Farokhzad, R. Margalit, R. Langer, *Nat. Nanotechnol.* **2007**, *2*, 751 – 760; b) J. Shi, A. R. Votruba, O. C. Farokhzad, R. Langer, *Nano Lett.* **2010**, *10*, 3223 – 3230; c) V. P. Torchilin, *Nat. Rev. Drug Discovery* **2005**, *4*, 145 – 160; d) Z. Gu, A. Biswas, M. Zhao, Y. Tang, *Chem. Soc. Rev.* **2011**, *40*, 3638 – 3655.

[9] a) F. M. Gribble, G. Loussouarn, S. J. Tucker, C. Zhao, C. G. Nichols, F. M. Ashcroft, *J. Biol. Chem.* **2000**, *275*, 30046 – 30049; b) M. W. Gorman, E. O. Feigl, C. W. Buffington, *Clin. Chem.* **2006**, *53*, 318 – 325; c) M. Leist, B. Single, A. F. Castoldi, S. Kuhnle, P. Nicotera, *J. Exp. Med.* **1997**, *185*, 1481 – 1486; d) T. W. Traut, *Mol. Cell. Biochem.* **1994**, *140*, 1 – 22.

[10] a) M. Naito, T. Ishii, A. Matsumoto, K. Miyata, Y. Miyahara, K. Kataoka, *Angew. Chem.* **2012**, *124*, 10909 – 10913; *Angew. Chem. Int. Ed.* **2012**, *51*, 10751 – 10755; b) S. Biswas, K. Kinbara, T. Niwa, H. Taguchi, N. Ishii, S. Watanabe, K. Miyata, K. Kataoka, T. Aida, *Nat. Chem.* **2013**, *5*, 613 – 620; c) R. Mo, T. Jiang, R. DiSanto, W. Tai, Z. Gu, *Nat. Commun.* **2014**, *5*, 3364, DOI: 10.1038/ncomms4364.

[11] a) C. C. Wu, T. Chen, D. Han, M. X. You, L. Peng, S. Cansiz, G. Z. Zhu, C. M. Li, X. L. Xiong, E. Jimenez, C. J. Yang, W. H. Tan, *ACS Nano* **2013**, *7*, 5724 – 5731; b) X. L. Zuo, S. P. Song, J. Zhang, D. Pan, L. H. Wang, C. H. Fan, *J. Am. Chem. Soc.* **2007**, *129*, 1042 – 1043; c) J. W. Liu, Y. Lu, *Adv. Mater.* **2006**, *18*, 1667 – 1671.

[12] a) J. B. Chaires, J. E. Herrera, M. J. Waring, *Biochemistry* **1990**, *29*, 6145 – 6153; b) V. Bagalkot, O. C. Farokhzad, R. Langer, S. Jon, *Angew. Chem.* **2006**, *118*, 8329 – 8332; *Angew. Chem. Int. Ed.* **2006**, *45*, 8149 – 8152; c) Z. Xiao, C. Ji, J. Shi, E. M. Pridgen, J. Frieder, J. Wu, O. C. Farokhzad, *Angew. Chem.* **2012**, *124*, 12023 – 12027; *Angew. Chem. Int. Ed.* **2012**, *51*, 11853 – 11857.

[13] a) L. R. Brewer, M. Corzett, R. Balhorn, *Science* **1999**, *286*, 120 – 123; b) F. L. Sorgi, S. Bhattacharya, L. Huang, *Gene Ther.* **1997**, *4*, 961 – 968.

[14] a) T. Jiang, Z. Zhang, Y. Zhang, H. Lv, J. Zhou, C. Li, L. Hou, Q. Zhang, *Biomaterials* **2012**, *33*, 9246 – 9258; b) S. Simões, J. N. Moreira, C. Fonseca, N. Düzgüneş, M. C. Pedroso de Lima, *Adv. Drug Delivery Rev.* **2004**, *56*, 947 – 965.

[15] a) S. Chono, S.-D. Li, C. C. Conwell, L. Huang, *J. Controlled Release* **2008**, *131*, 64 – 69; b) N. Toriyabe, Y. Hayashi, H. Harashima, *Biomaterials* **2013**, *34*, 1337 – 1343; c) K. Kogure, R. Moriguchi, K. Sasaki, M. Ueno, S. Futaki, H. Harashima, *J. Controlled Release* **2004**, *98*, 317 – 323.

[16] a) W. Liang, T. Levchenko, V. Torchilin, *J. Microencapsulation* **2004**, *21*, 251 – 261; b) D. D. Verma, T. S. Levchenko, E. A. Bernstein, V. P. Torchilin, *J. Controlled Release* **2005**, *108*, 460 – 471.

[17] a) Y. Obata, S. Tajima, S. Takeoka, *J. Controlled Release* **2010**, *142*, 267 – 276; b) K. Kono, M. Iwamoto, R. Nishikawa, H. Yanagie, T. Takagishi, *J. Controlled Release* **2000**, *68*, 225 – 235;

 © 2014 Wiley-VCH Verlag GmbH & Co. KGaA, Weinheim

c) A. El-Sayed, I. A. Khalil, K. Kogure, S. Futaki, H. Harashima, *J. Biol. Chem.* **2008**, *283*, 23450 – 23461.

[18] a) R. Mo, Q. Sun, J. Xue, N. Li, W. Li, C. Zhang, Q. Ping, *Adv. Mater.* **2012**, *24*, 3659 – 3665; b) K. Shigeta, S. Kawakami, Y. Higuchi, T. Okuda, H. Yagi, F. Yamashita, M. Hashida, *J. Controlled Release* **2007**, *118*, 262 – 270.

[19] a) E. K. Chow, D. Ho, *Sci. Transl. Med.* **2013**, *5*, 216rv214; b) M. G. Vander Heiden, *Nat. Rev. Drug Discovery* **2011**, *10*, 671 – 684; c) L. Galluzzi, O. Kepp, M. G. Vander Heiden, G. Kroemer, *Nat. Rev. Drug Discovery* **2013**, *12*, 829 – 846; d) W. R. Wilson, M. P. Hay, *Nat. Rev. Cancer* **2011**, *11*, 393 – 410.

 © 2014 Wiley-VCH Verlag GmbH & Co. KGaA, Weinheim